A simplified model of uniform shading in large photovoltaic arrays

Chris Deline, Aron Dobos, Steven Janzou
National Renewable Energy Laboratory
Jenya Meydbrey, Matt Donovan
PV Evolution Labs

Abstract:

This work presents a novel analytical approximation of the effect of inter-row shading on large photovoltaic (PV) arrays. Computation time is greatly reduced relative to full numerical simulations, allowing this method to be used in annual production estimation software- for instance, it is currently implemented in the National Renewable Energy Laboratory's System Advisor Model program. Comparison with full I-V curve simulations indicate that this simplified approach has typical error of 1% over multiple module fill factor, shade extent and shade opacity assumptions. Maximum error of 2%-6% was found for simulations of crystalline silicon modules. Comparison with experimental results shows good agreement between the experiment and the model for both large PV systems with small amounts of shade, and small systems with large amounts of shade, thus highlighting this model's broad range of applicability.

Keywords: Photovoltaic modeling; partial shading; inter-row shading; annual performance model;

1. Introduction

Photovoltaic (PV) arrays for commercial power production are becoming more widespread, with an eventual goal of competing with non-renewable sources of electricity generation. As costs for individual PV system components decrease—including reduced costs for PV panel and balance of system components—land-related costs can become a critical element of the system budget, as shown in Pera et al., 2011. Other constraints such as limited rooftop space can also motivate high-density PV system designs. In such situations, it is possible that partial shading from surrounding obstructions and self-shading from adjacent rows can lead to power losses at certain times of the day, yet still be an economical solution due to other financial considerations. In order to understand the performance tradeoffs under such intentional shading situations, accurate performance modeling is required, including modeling the impact of partial shading.

Models of partial shading loss have existed for over 40 years (Rauschenbach, 1971), with accurate computer simulations becoming possible more recently (Bishop, 1988; Quaschning and Hanitsch, 1996; King, 1996). With faster computers, calculations of the impact of various shading situations on PV panels have been published many times (Kawamura et al., 2003; Alonso-Garcia, Ruiz and Hermann, 2006; Karatepe et al., 2007) and confirmed against experimental results (Woyte et al., 2003; Alonso-Garcia, Ruiz and Chenlo, 2006; Deline, 2009). Many of these computer simulations are high-accuracy cell-level models that sum the forward- and reverse-bias current-voltage (I-V) characteristics of shaded and unshaded solar cells, providing the ability to simulate an arbitrary shading condition and array configuration. However, computation speed is sacrificed to achieve this accuracy and using such a linear approach to simulate a large PV installation with thousands of panels and hundreds of thousands of individual cells requires long simulation times. Additional approaches have therefore been considered to reduce simulation times or to specifically investigate large PV installations; these include Monte Carlo techniques in Iannone et al., 1998 and analytical models (Petrone et al., 2007; Thakkar et al., 2010; Brecl and Topic, 2011). A new analytical approach is proposed here with the necessary flexibility, speed, and

accuracy to be used in annual PV yield simulation software such as the National Renewable Energy Laboratory's (NREL) System Advisor Model (SAM) (Blair et al., 2008), or other proprietary simulations. Such simulation applications require a shading algorithm to have the flexibility to handle a wide variety of PV panel technologies and fill factors, and the speed to allow hourly performance calculations capturing thousands of different irradiance and shade patterns. Additionally, these software packages are typically run on conventional computers with required simulation times on the order of seconds to simulate an entire year of PV production. These constraints indicate the need for a simplified analytical shade model rather than a complete numerical simulation.

In this work, we first describe a reference approach to modeling inter-row partial shading, providing full I-V curve simulation of inter-row shading patterns, but with long simulation times. We then propose a second model: a novel, simplified analytical approximation that allows faster computation but is limited in scope to primarily inter-row shading conditions, where shading occurs regularly throughout the system. Results from the full simulation are compared with those from the simplified model to estimate the uncertainty of the new model. Additionally, results from the simplified model are compared with experimental results to verify the accuracy of the method.

2. Modeling details

2.1 Model scope and simplifying assumptions

The analytical shade analysis proposed here is based on several simplifying assumptions, as described in Figure 1. The first assumption is that a single solar panel is composed of several submodules, each protected by a single bypass diode, and connected in series within the panel. This is the typical scenario for, e.g., a 60-cell silicon solar panel, where 20 solar cells make up a submodule, which is protected by one of the three bypass diodes in the solar panel. More complicated panel configurations where a single cell can belong to multiple submodules, or where cells are cross-tied or placed in parallel are not considered here. This assumption is more appropriate for estimating shading loss in conventional panels rather than monolithically integrated thin-film modules with cells extending the width of the module.

A second simplifying assumption is that each of the parallel strings of panels in the large PV installation contains the same percentage of shaded submodules. Therefore, for the fraction of shaded parallel strings in the system X, the fraction of shaded submodules S is constant. While this assumption is not flexible enough to model irregular shading patterns, it is sufficient for the case of inter-row shading where shading occurs regularly throughout the system.

A third simplification is that partial shading on a given submodule can be dealt with in a binary fashion. Previous studies have shown that shading on just a single cell in a submodule can produce a similar current-voltage (I-V) characteristic to the entire submodule being uniformly shaded (Paraskevadaki and Papathanassiou, 2011; Deline, 2009). In this study, the shaded I-V curve is assumed to be consistent with shading of the entire submodule. This assumption will be verified through comparison with cell-level simulations in Section 2.3.1 below.

A final point is that this model deals specifically with performance reduction due to the loss of direct-beam irradiance. Reduction in diffuse and reflected components of irradiance due to, e.g., horizon blocking have been dealt with elsewhere, in e.g. Applebaum and Bany, 1979 and will not be covered here, although their impact would factor into any calculation of shaded PV performance.

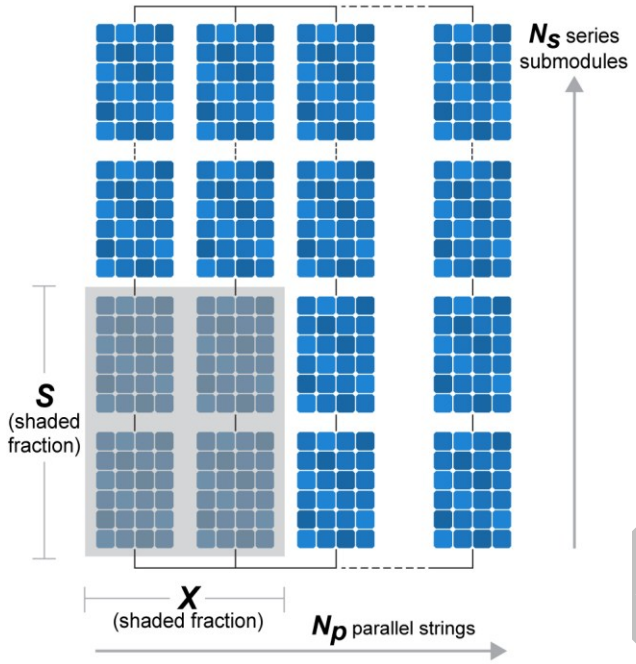

Figure 1: Illustration of the simplifications used to limit this simulation. *S* indicates the fraction of modules (or submodules) in a series string experiencing shading, where the beam component of irradiance is completely blocked. *X* indicates the fraction of parallel strings experiencing this uniform shading. Note that *S* is the same for each shaded row in this simplified approach.

2.2 Inter-row-shading full I-V reference model

We begin by discussing the reference model used to validate the analytical approach. This detailed reference case follows the conventional I-V curve summing approach of previous publications. The reference model determines both shaded and unshaded submodule I-V curves, then sums them to create cell-, string-, and system-level I-V curves for a given shade configuration.

Individual module I-V curves are generated using the five-parameter I-V curve equation of deSoto, Klein and Beckman, 2006:

$$I = I_{ph} - I_{sat} \exp\left(\frac{V + IR_s}{a} - 1\right) - \frac{V + IR_s}{R_{sh}} \quad (1)$$

where I_{ph}, I_{sat}, R_s, R_{sh} and a represent the diode light current, reverse saturation current, series resistance, shunt resistance and diode ideality factor, respectively. Parameters for specific modules at standard test conditions (STC) are found in the California Energy Commission (CEC) PV module database, duplicated in the SAM program. Submodule I-V curves are derived from the module curves of Eq (1) by dividing voltage by the number of bypass diodes. Cell-level I-V curves are further derived by dividing voltage by the number of cells per submodule.

To account for the presence of bypass diodes in each submodule, an ideal diode (Shockley, 1949) is assumed in parallel with the submodule with saturation current $I_0 = 8 \times 10^{-9}$ and a forward voltage of V_d = 0.5 V. For cell-level simulations, reverse-bias cell behavior is modeled according to Bishop, 1998.

To calculate partially shaded performance of submodules or cells, new parameter values for Eq (1) are calculated based on the method of deSoto, Klein and Beckman, 2006 assuming constant temperature and a reduced irradiance fraction E_e. E_e is calculated for the shaded module by removing the beam component of irradiance G_b from the total plane of array irradiance, or

$$E_e = \frac{G_r + G_d}{G} \quad (2)$$

where the total incident irradiance $G = G_d + G_r + G_b$ is composed of diffuse, ground-reflective, and beam irradiance components, respectively.

Once obtained, cell-level I-V curves are scaled in voltage, proportional to the number of shaded or unshaded cells in the submodule to obtain both shaded and unshaded cell I-V curves. The two scaled I-V curves are summed together by adding linearly interpolated voltages at 200 current points between 0 A and I_{sc} of the unshaded cell, resulting in the I-V curve of a partially shaded submodule.

Submodule I-V curves are similarly scaled in voltage by SN_s for the shaded submodule, and (1-S)N_s for the unshaded submodule, where S is the fraction of shaded submodules in the series string, and N_s is the number of series submodules in the string. Interpolated submodule voltage points are summed at current points between 0A and I_{sc} to generate string-level I-V curves.

The shaded string curve is scaled in current by XN_p, and the unshaded string curve is scaled by (1-X)N_p where X is the fraction of shaded parallel strings and N_p is the number of parallel strings in the system. The system curve is the sum of interpolated currents of the two scaled string I-V curves at voltage points between 0 V and the unshaded string's V_{oc}. System peak power accounting for shade, Ps_{ys}, is determined by the maximum of the reference simulation power-voltage curve. Unshaded peak power of the system is defined as P_{Sys0} (subscript 0 indicates unshaded conditions herein).

2.3 Proposed simplified analytical model

An analytical model to replace the above approach is obtained through a number of approximations depending on four variables: 1) fraction of submodules shaded in a string S; 2) fraction of parallel strings shaded X; 3) irradiance fraction reaching the shaded submodule E_e; and 4) submodule fill factor FF_0, defined by the nameplate parameters $FF_0 = P_{mp0} / V_{oc0} / I_{sc0}$. The basic framework of the model is to look at the reduced performance of a partially shaded string P_{Str}/P_{Str0} with respect to the four variables (S, X, E_e, FF_0). The system power can then be determined by summing the power of the shaded and unshaded strings:

$$P_{Sys}/P_{Sys0} = X(P_{Str}/P_{Str0}) + (1 - X) \quad (3)$$

In using this convention, all the performance losses in the system are accumulated and divided among the shaded strings, even if the voltage mismatch causes some of the unshaded strings to operate off of their peak power operating point. In this analysis, unshaded strings count for their full peak power. This is merely an accounting convention with no impact on simulation accuracy. If unshaded strings do experience a loss in power, that power loss is attributed to the shaded strings for the sake of convenience, as per Eq (3).

2.3.1 Analytical model – Small S, X condition

The first equation in determining P_{Str}/P_{Str0}comes from conceptually examining the case of only one parallel string experiencing opaque shade in a large PV installation. This simplification allows one to assume that the operating voltage of the system is the same as under unshaded conditions = N_s V_{mp0} where N_s is the number of submodules in a series string, and V_{mp0} is the submodule peak-power voltage.

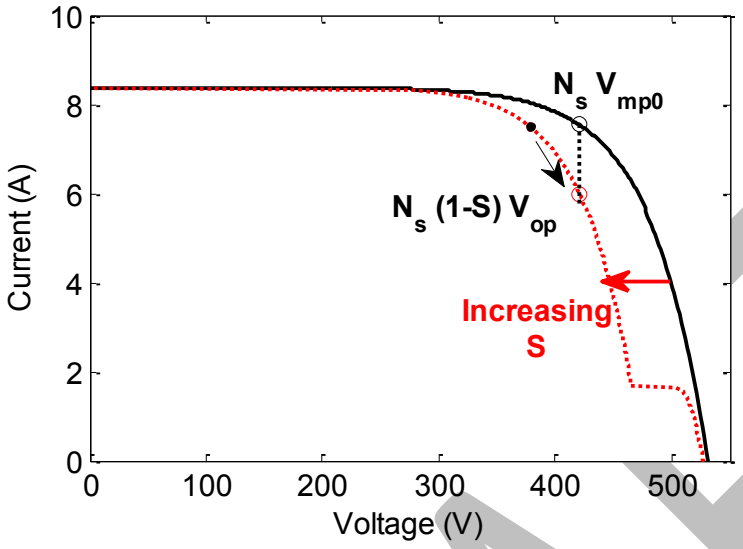

Figure 2: Partially shaded string I-V curve (red dashed) showing a reduced operating current with increased substring shading *S* relative to the unshaded I-V curve (black line). With constant operating voltage, the shaded string operates at a higher voltage and lower current (red circle) than its local maximum power point (black dot).

If one or more substrings are shaded, the operating voltage of the string is the same, but the number of substrings contributing to the string voltage is reduced, due to bypass diode turn-on, as shown in Figure 2. Therefore, the operating voltage of each unshaded panel in the shaded strings increases. The operating voltage of each unshaded submodule in the shaded string, V_{op}, is:

$$V_{op} = \left(\frac{V_{mp0}}{1-S}\right) \tag{4}$$

with the assumption that V_{op} for shaded submodules = 0 due to bypass diode operation. The power of the shaded string P_{Str} is equal to the fraction of unshaded submodules in that string, multiplied by the submodule operating voltage and the current at that operating voltage $I(V_{op})$:

$$P_{Str} = (1-S)N_s V_{op} I(V_{op}) = N_s V_{mp0} I(V_{op}) \tag{5}$$

The string power decreases more rapidly with shading for high-FF_0 panels. This is illustrated in a plot of P_{Str}/P_{Str0} vs. *S* for different PV panels, shown in Figure 3. Three panels are shown with a range of FF_0: SunPower SPR-230 (FF_0 = 0.79), Kyocera KD-205 (FF_0 = 0.74), and a CIGS panel, Solar Frontier SF-165 (FF_0 = 0.68).

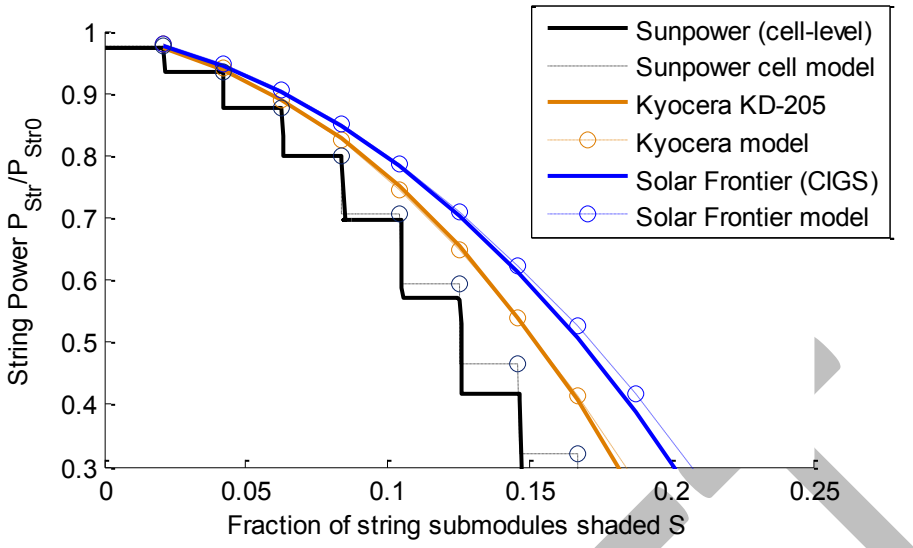

Figure 3: String power derating curves for select panels, from the reference I-V simulation (lines). 80% opaque shading is assumed (E_e = 0.2), and minimal parallel string shading (X = 0.1). Submodule model results (open circles) are based on Eq. **6** - (**8**). Cell-level results are indicated for the SunPower module. Kyocera and Solar Frontier results assume an infinite series string of modules.

If an infinite number of series-connected modules are assumed in a string, smooth curves are obtained, as shown for the Kyocera and Solar Frontier modules in Figure 3. In the case of a finite number of modules, cell-level effects of partial shading become apparent, as represented by the SunPower module[1]. For the cell-level analytical model, it is assumed that a slight increment of shading on a given submodule causes that submodule to be fully shaded, resulting in a discrete drop in production. This assumption lines up closely with the reference simulation, where a shadow covering one cell is sufficient to drive that cell far enough into reverse bias to cause the protecting bypass diode to begin conducting. This also results in a discrete drop in production, equivalent to that submodule being completely shaded. It is sufficient, therefore, to only consider conditions where S moves in discrete steps of $1/N_s$ (open circles in Figure 3), i.e. partially shaded submodules are considered to be fully shaded. An analytical equation that describes the smooth (fully-shaded submodule) curves of Figure 3 is given by a second-order polynomial fit:

$$\frac{P_{Str}}{P_{Str0}} = 1 - C_1 S^2 - C_2 S \tag{6}$$

Two fitting coefficients are required for the analytical fit: C_1 and C_2. These coefficients were determined by least-squares regression to multiple iterations of the reference I-V model at different FF_0 and X:

$$C_1 = (109\, FF_0 - 54.3)\mathrm{e}^{-4.5\,X} \tag{7}$$

$$C_2 = -6\,X^2 + 5\,X + 0.28 \quad [X \in 0..0.65]$$
$$C_2 = 1 \quad [X \in 0.65..1] \tag{8}$$

[1] SunPower's cells in actuality are peculiar due to their very low reverse-bias breakdown voltage, which is not fully captured in this analysis for simplicity's sake.

Examples of these analytic approximations for X = 0.1 are shown in Figure 3 along with curves determined from the full reference simulation.

2.3.2 Analytical model – Large X condition

The analysis of *2.3.1* assumes that a small fraction of parallel strings experience shading. With more parallel shaded strings (larger *X*), the assumption of a constant operating voltage is increasingly violated. In fact, for *X* = 1, the shading simulation approaches a new conceptual limit- one in which the global V_{mp} coincides with the V_{mp} of the shaded strings, rather than the V_{mp} of unshaded strings. Referring back to Figure 2 and Eq. (5), the submodule operating voltage V_{op} and $I(V_{op})$ are set equal to V_{mp0} and I_{mp0}, respectively. For *X* = 1, Eq. (5) reduces to:

$$\frac{P_{Str}}{P_{Str0}} = \frac{P_{Sys}}{P_{Sys0}} = 1 - S \quad (\text{for X} = 1) \tag{9}$$

A more accurate analysis also includes the power loss from the bypass diodes active in the shaded submodules:

$$\frac{P_{Str}}{P_{Str0}} = 1 - S - \frac{P_{diode}}{P_{Str0}} = \frac{P_{Sys}}{P_{Sys0}} \tag{10}$$

where P_{diode} is the power loss in a string's bypass diodes $= V_d I_{mp0} S N_s$.

Now substituting P_{Sys}/P_{Sys0} into Eq. (3) with $X \neq 1$ and canceling terms:

$$\frac{P_{Str}}{P_{Str0}} = \frac{X - S\left(1 + \frac{V_d}{V_{mp0}}\right)}{X} \tag{11}$$

where V_d is the reverse voltage of the diode, and V_{mp0} is the submodule peak operating voltage.

Equation (11) provides a second limit condition for P_{Str}/P_{Str0} occurring at large *X*, while Eq. 6 is valid for small *X*. For any given in-between *X*, the modeled results take the maximum of Eq. (6) or Eq. (11).

An example of this modeled behavior is shown in Figure 4 for a Kyocera KD-205 panel. For X = 0.1, the modeled and reference results are equivalent to those given previously in Figure 3. At *X* = 0.5, the model still follows Eq. (6), but by *X* = 1, Eq. (11) provides the maximum P_{Str}/P_{Str0} and is chosen instead.

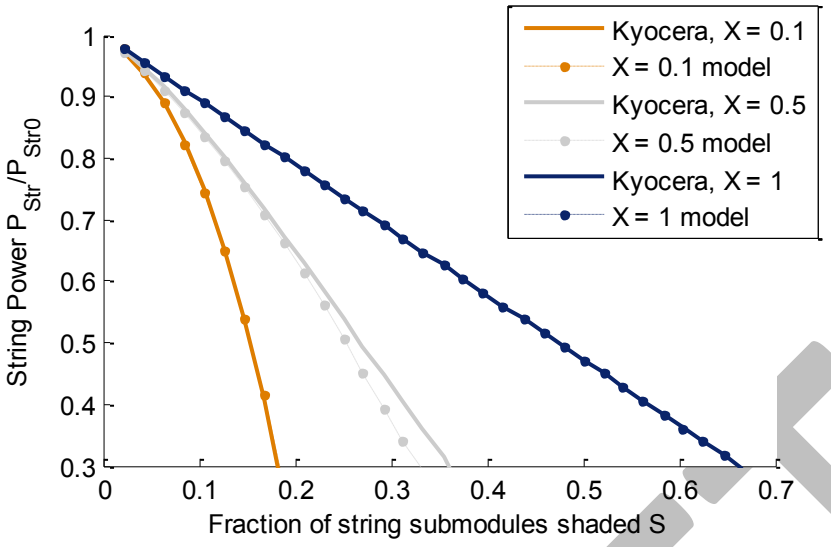

Figure 4: String power derating curves for BP365 panel, from full I-V simulation reference (lines). Multiple shaded strings are assumed (X = 0.1, X = 0.5 and X = 1) with 80% opaque shading. Modeled results (dots) are based on Eq. (**6)** - (11).

2.3.3 Analytical model – Large S condition

A third conceptual limit is required to complete the analytical model of uniform shading: a large S limit. Both Alonso-Garcia et al., 2006, and Paraskevadaki and Papathanassiou, 2011 have shown that two local maxima exist in shaded system power-voltage curves: a low-voltage operating point, and a high-voltage operating point. With large S, the global maximum coincides with the high-voltage, low-current operating point. This occurs if the shading is not entirely opaque and the global maximum current is equal to I_{mp} N_s (shaded submodule current times each submodule N_s) rather than relying on bypass diodes to operate the string at I_{mp0} N_s (1-S). This is illustrated by a close-up of the power vs. voltage curve in Figure 5 at different submodule shade conditions.

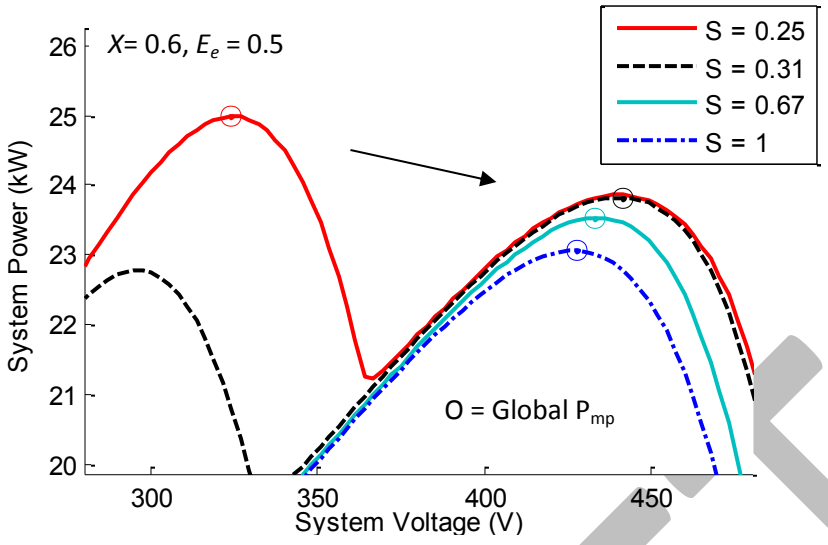

Figure 5: Close-up of system power vs. voltage curve for Kyocera panels showing alternate high-voltage peak power operating point with *S* > 0.25. System power becomes limited by the shaded string as $\boldsymbol{P_{Str}/P_{Str0} => E_e}$ when *S* = 1. System configuration: 16 series panels, 10 parallel strings.

As shown in Figure 5, with increased shading *S*, the global maximum switches from a low to a high-voltage local operating point, then continues to decrease in power with *S*, until it reaches a minimum at *S* = 1. The operating point at *S* =1 coincides approximately with shaded submodule power $P_{mp}/P_{mp0} = E_e$. This sets a lower limit of $P_{Str}/P_{Str0} = E_e$ for *S* = 1. Figure 6 shows details of the reference simulation for P_{Str}/P_{Str0}, particularly at large E_e. The main feature of this plot is that for small *S*, P_{Str}/P_{Str0} follows Eq. (6) until it approaches $P_{Str}/P_{Str0} \approx E_e$. The global maximum then changes to the alternate V_{mp} operating point (as shown in Figure 5) and follows a linear decrease until $P_{Str}/P_{Str0} = E_e$ at *S* = 1. The linear decrease can be understood by referring back to Figure 5, which shows that system power decreases slowly from *S* = 0.31 to *S* = 1. This decrease is represented by the slope in the P_{Str}/P_{Str0} curve of Figure 6.

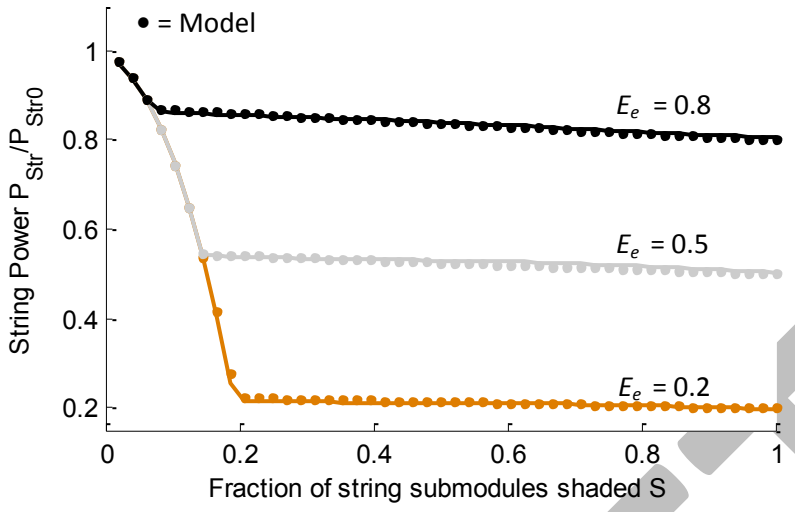

Figure 6: String power derating curve for Kyocera KD-205 panel, showing alternate operating point near $\boldsymbol{P_{Str}/P_{Str0} = E_e}$. Results shown for X = 0.1 and multiple E_e conditions.

An empirical model for P_{Str}/P_{Str0} is created for the high S limit, which is represented by a straight line with intercept E_e at S = 1. A constant term C_3 is used for the slope of this straight line, leading to the equation:

$$\frac{P_{Str}}{P_{Str0}} = C_3(S-1) + E_e \tag{12}$$

An upper limit condition to C_3 can be determined by the observation that at S = 0, $P_{Str}/P_{Str0} = 1$. Therefore, substituting into Eq. (12) yields:

$$C_3 = \max\left[(C_{3,0})\,;(E_e - 1)\right] \tag{13}$$

where $C_{3,0}$ is the best-fit slope in the linear (large-S) portion of Figure 6. The slope $C_{3,0}$ is a negative value and was found for the multiple modules considered here to depend on FF_0, E_e and X:

$$C_{3,0} = (-0.05E_e - 0.01)X + (0.85\,FF_0 - 0.7)E_e - 0.085\,FF_0 + 0.05 \tag{14}$$

The final analytical model therefore takes the maximum of the three limit condition equations:

$$\frac{P_{Str}}{P_{Str0}} = \max[\text{Eq. (6)}; \text{Eq. (11)}; \text{Eq. (12)}] \tag{15}$$

and uses this value in Eq. (3) to determine the overall performance reduction due to shade.

2.4 Error analysis

A thorough comparison was conducted of the full reference simulation with its analytical approximation. In particular, several detailed error plots were constructed for a simulated array field with 100 parallel strings of 16 panels in series, using reference I-V curves for a SunPower SPR-230 module. Shade opacity is assumed to be 30% (E_e = 0.3) since this resulted in a maximum in error for this module. Figure 7 displays the conditions under which the various limit equations of Eq. (15) occur. The large S limit [Eq. (12)] predominates when S is greater than a value of 0.2–0.6. This threshold value is dependent on the

shade opacity E_e, with low E_e values (more opaque shading) shifting the onset of Eq. (12) to higher S conditions. The large X limit [Eq. (11)] only occurs for $X > 0.4$ and when the large S limit does not apply.

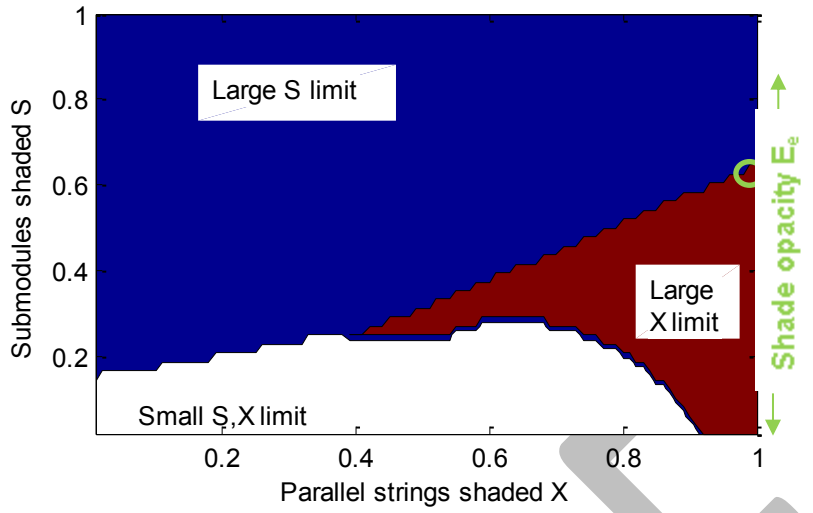

Figure 7: Shading conditions when the large X limit (Eq.11) and large S limit (Eq. 12) apply. Otherwise the small S,X limit (Eq.**6**) applies. This plot is for the SunPower SPR-230 panel with E_e = 0.3. The green circle to the right of the plot indicates the division between large X and S conditions, which is set by E_e.

The various limit conditions in Figure 7 are useful in explaining the distribution of errors between the full reference simulation and the simplified analytical simulation, because a majority of errors are concentrated near the divisions between the three limit equations. Figure 8 shows the difference in P_{Sys} between the analytical and reference models, calculated as $P_{Sys,Analytical}$ / $P_{Sys,Ref}$. Error is less than 1% for a majority of X and S simulation conditions, with a maximum absolute error of 4.4% occurring at the interface of the three limit equations.

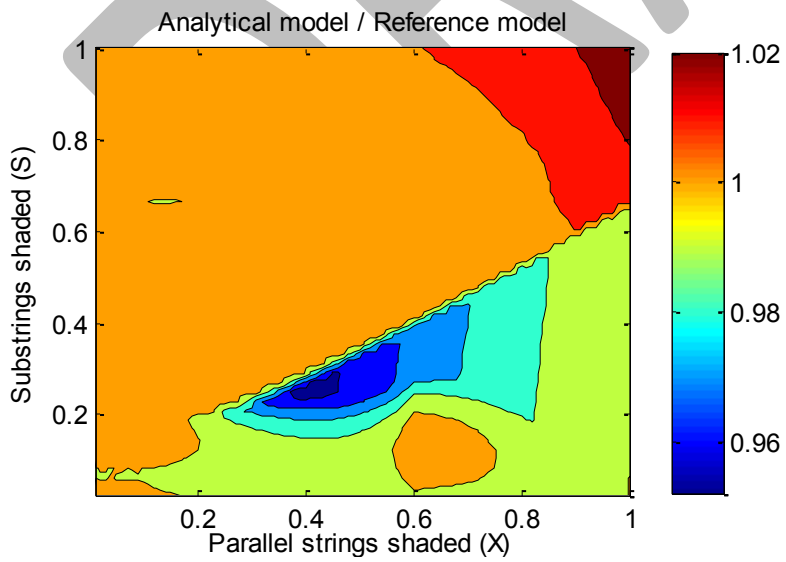

Figure 8: Difference in output between analytical model and full IV curve reference model. The simplified model under-predicts system power by a maximum of 4.4% for a SunPower system, with E_e = 0.3.

To highlight the broad applicability of the model, a series of comparisons were made, recording the maximum absolute error between the analytical model and the reference simulation over a range of diffuse irradiance conditions (E_e from 0.1 to 0.9) and for a number of different PV panels in the CEC database. These results are given in Figure 9. Detailed error plots are similar to that of Figure 8 in that the maximum error occurs under specific shading conditions, so the average error for these panels is much lower. The panels with lower FF_0 tend to display greater modeling error, as do all panels at lower E_e. For all standard silicon panels investigated, the maximum model error was 6% or less for all shade conditions.

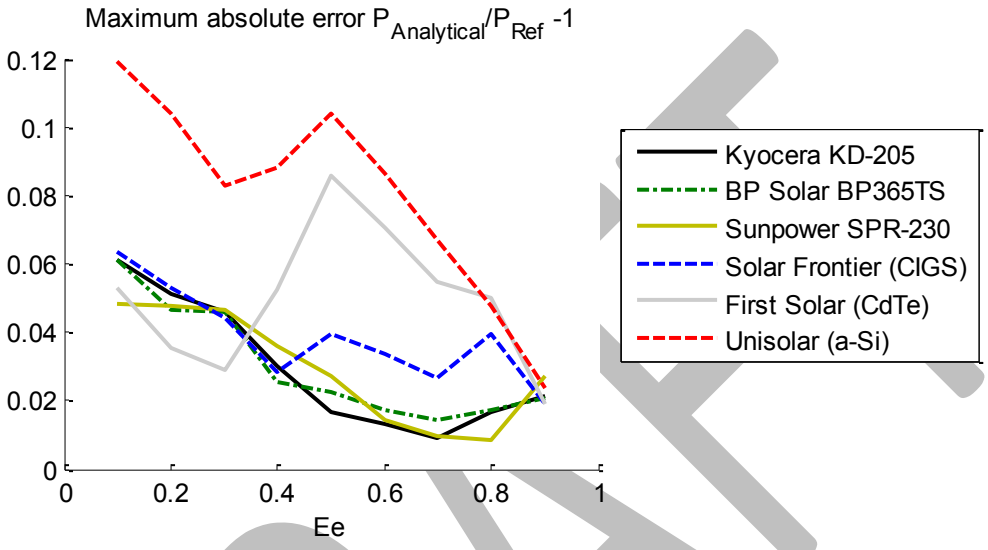

Figure 9: Maximum absolute error in system power measurement ($P_{Sys,Analytical}$ / $P_{Sys,Ref}$) -1 for all *S, X* and E_e. Low FF_0 panels (First Solar, Unisolar) tend to have greater error, as do panels at lower E_e.

3. Experimental verification of simulations

Field measurements were collected to validate the analytical model presented here. Two separate PV systems were instrumented to determine shading impact: a small 8.5-kW system composed of three parallel strings as described in Deline et al., 2012, and a large 600-kW system composed of 198 parallel strings. In the first system, artificial shading is applied in varying amounts by drawing a black mesh fabric across the array. In the second PV system, a nearby light pole casts a large shadow across the array throughout the day. Both systems are instrumented to determine the power loss in the shaded strings with varying amounts of system shade.

Test Array 1 consists of three parallel strings of 12 panels. The 36 Sharp NU-U235 panels were tested indoors at STC and found to have an average FF_0 of 0.735. The panels are connected to a Fronius IGPlus 11.4-3 inverter, with the inverter output monitored by a revenue-grade (0.2% accuracy) Shark 100T power transducer. Meteorological data such as plane of array (POA) irradiance were monitored using a silicon reference cell, and panel temperature using thermocouples.

Figure 10: Shading fabric with 37% transmittance, drawn across Test Array 1.

Per-panel shading is applied to the system using a black vinyl/polyester mesh fabric (Figure 10). A transmittance of 37% was determined by spectral transmittance measurement from 400 nm to 1100 nm, corrected to the ASTM G173 global reference spectrum. Data are collected on two sequential sunny days, with the system operating without shading on the first day, and operating under different shading conditions on the second day. Shading conditions with X = 0.66 and X = 1 are accomplished by simultaneously shading either two out of three parallel strings, or all three parallel strings, respectively. Conditions from S = 0 to S = 0.5 are accomplished by sequentially drawing the shading fabric across equal numbers of the PV panels in either two or all three of the parallel strings. With three submodules per PV panel and the panels deployed in portrait orientation, the shading fabric is deployed from left to right in increments of 1/3 of a panel, with the fabric covering the entire height of the panel. Because the transmittance of the fabric is 37%, the simulated E_e irradiance condition is 0.37.

For each of the shading conditions considered, AC kWh production is monitored over a 15-minute interval. Data is collected under clear-sky conditions with POA irradiance > 500 W/m^2. For each shade condition, the value of system AC performance is recorded and referenced to the unshaded AC performance at the same time of day on a previous day. Changes in panel temperature and irradiance are corrected back to STC by the translation coefficients of Marion, 2008.

Test Array 2 is a large commercial array composed of Evergreen ES-190 panels (FF_0 ≈ 0.7). Natural shading exists on this array due to a series of light poles located in front of the array. As the shadow moves throughout the day, different strings are shaded to different extents (Figure 11). With 198 parallel strings, only a few of which are shaded, the shading on the system is minor, and X ≈ 0. Individual string currents are monitored using split-core Hall-effect sensors. Two sensors are placed on unshaded strings, and two sensors are placed on shaded strings, determining the relative reduction in string current due to shading. Because the strings are all in parallel, voltage is the same, and reduced string power P_{str} / P_{str0} equals the ratio of string currents I_{str} / I_{str0}. Shadows occur in the morning when global horizontal irradiance G > 300 W/m^2 and E_e < 0.25. Comparison with the empirical shade model is not perfect in this test array because shading does not cover a significant fraction of each submodule; in some cases, the narrow pole shadow only crosses one or two cells in a submodule.

Figure 11: A nearby shading obstruction (light pole) casts a shadow across Test Array 2.

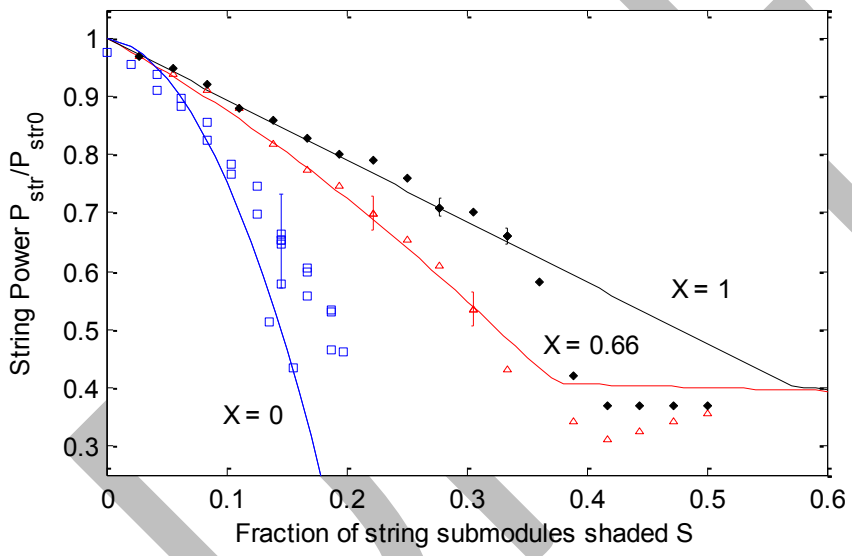

Figure 12: Comparison of empirical model results (solid lines) with experimental data (points). $X = 0$ data from large PV system with natural shading ($E_e < 0.25$). $X = 0.66$ and $X = 1$ data from 3-string system, with artificial shading ($E_e = 0.37$).

The agreement of experimental results with the empirical method is generally good, particularly for Test Array 1, where shading covers all of a submodule rather than just a few cells. Some difference exists between the model and experiment for the $X = 0$ data, possibly because of the irregular extent of the shadow across each submodule.

Additional differences between the empirical model and experiment can be seen with large shade extent ($S > 0.3$). Particularly in the $X = 1$ case, a steep drop in string power is visible at $S = 0.37$. The reason for this drop is due to the nonideal nature of real PV inverters; the inverter is operating at its minimum DC input voltage starting at $S = 0.3$. With further shading, the global maximum operating voltage lies below the inverter's minimum operating voltage. By $S = 0.42$ the inverter has switched to an alternate high-

voltage, low-current operating point, which coincides with the large-*S* limit of Eq. (12). This sort of nonideal inverter behavior is unaccounted for in the analytical method presented here.

A second slight difference can be seen between the simulation model and the experimental results that may be attributed to the experiment setup. The mesh fabric used for shading in the $X = 1$ and $X = 0.66$ cases was tested to have a transmittance of 37% when the light is directly normal to the fabric. Under actual test conditions, the incidence angle of the sunlight was not normal to the test array, and further reduction in transmittance may have occurred, which could account for the lower-than-expected system performance for $S = 0.4–0.5$.

4. Conclusion

An analytical approximation has been developed to represent the performance impact of partial shading on a large PV system. Simple empirical equations are used to allow fast computation consistent with the requirements of annual performance estimation software such as NREL's SAM. As a result, an electrical model of partial shading can be used rather than simpler and less accurate linear shade approximations. To determine the reduced performance of a single shaded string, three equations are combined to create the analytical estimate: an equation assuming small amounts of shade, one assuming large numbers of parallel shaded strings (large *X*), and one assuming a large percentage of submodules shaded per string (large *S*). The maximum of the three equations is used, resulting in an analytical approximation of shaded system performance that is valid over any shade condition, for panels of any fill factor.

Through a comparison with a full I-V curve simulation, the simple analytical model was verified to have small error (<1%) over a majority of the simulation space, with maximum error of 2%–6% for conventional panels. Cell-level I-V curve simulations justify a simplification in the model that partly shaded submodules be treated as fully shaded.

A comparison with field experiments found the analytical model to predict power losses from shadows in both large systems with small amounts of shade, and small systems with large amounts of shade. Real-world equipment limitations including low-voltage operation limits of PV inverters are not included in this model and may introduce additional uncertainty. However, for the case of uniform shading as would arise from inter-row shading, this model has been demonstrated to accurately predict system performance under a wide variety of conditions.

Acknowledgement

This work was supported by the U.S. Department of Energy under Contract No. DE-AC36-08-GO28308 with the National Renewable Energy Laboratory. Helpful comments were provided by Cliff Hansen at Sandia National Labs and Sara MacAlpine at the University of Colorado.

References

Alonso-Garcia, M.C., Ruiz, J.M., Chenlo, F., 2006. Experimental study of mismatch and shading effects in the I-V characteristic of a photovoltaic module. Solar Energy Materials & Solar Cells **90**, 329-340.

Alonso-Garcia, M.C., Ruiz, J.M, Hermann, W., 2006. Computer simulation of shading effects in photovoltaic arrays. Renewable Energy **31**, 1986-1993.

Appelbaum, J., Bany, J., 1979. Shadow effect of adjacent solar collectors in large scale systems. Solar Energy **23**, 497-507.

Bishop, J.W., 1988. Computer simulation of the effects of electrical mismatches in photovoltaic cell interconnection circuits. Solar Energy Mater. Solar Cells **25,** 73-89.

Blair, N., Mehos, M., Christensen, C., Cameron, C., 2008. Modeling Photovoltaic and Concentrating Solar Power Trough Performance, Cost, and Financing with the Solar Advisor Model. Proceedings of SOLAR 2008 - American Solar Energy Society, San Diego, California. See also https://sam.nrel.gov/

Brecl, K., Topic, M., 2011. Self-shading losses of fixed free-standing PV arrays. Renewable Energy **36**, 3211-3216.

Deline, C., 2009. Partially shaded operation of a grid-tied PV system. IEEE Photovoltaic Specialists Conference, Philadelphia, PA.

Deline, C., Meydbray, J., Donovan, M., Forrest, J., 2012. Photovoltaic Shading Testbed for Module-Level Power Electronics. NREL technical report NREL/TP-5200-54876.

De Soto, W., Klein, S.A., Beckman, W.A., 2006. Improvement and validation of a model for photovoltaic array performance. Solar Energy **80**, 78-88.

Iannone, F., Noviello, G., Sarno, A., 1998. Monte Carlo techniques to analyse the electrical mismatch losses in large-scale photovoltaic generators. Solar Energy **62**, 85-92, 1998.

Karatepe, E., Boztepe, M., Colak, M., 2007. Development of a suitable model for characterizing photovoltaic arrays with shaded solar cells. Solar Energy **81**, 977-992.

Kawamura, H., Naka, K., Yonekura, N., Yamanaka, S., Kawamura, H., Ohno, H., Naito, K., 2003. Simulation of I-V characteristics of a PV module with shaded PV cells. Solar Energy Materials & Solar Cells **75,** 613-621.

King, D.L., Dudley, J. K., Boysen, W. E., 1996. PVSim: a simulation program for photovoltaic cells, modules and arrays. 25th IEEE Photovoltaic Specialists Conference, Washington, DC.

Marion, B., 2008. Comparison of Predictive Models for Photovoltaic Module Performance Equation (2). 33rd IEEE Photovoltaic Specialists Conference, San Diego, CA.

Pera, D., Brito, M., Maia Alves, J., Serra, J., Silva, C., Vallera, A. 2011. Optimization model for high density photovoltaic power plants by maximization of the return on investment. 26th Eurpoean Photovoltaic Solar Energy Conference and Exhibition, Hamburg-Germany.

Paraskevadaki, E. V., Papathanassiou, S. A., 2011. Evaluation of MPP Voltage and Power of mc-Si PV modules in partial shading conditions. IEEE Transactions on Energy Conversion **26**, 923-932.

Petrone, G., Spagnuolo, G., Vitelli, M., 2007. Analytical model of mismatched photovoltaic fields by means of Lambert W-function. Solar Energy Materials & Solar Cells **91**, 1652-1657.

Quaschning, V., Hanitsch, R. 1996. Numerical simulation of current-voltage characteristics of photovoltaic systems with shaded solar cells. Solar Energy **56,** 513-520.

Rauschenbach, H.S., 1971. Electrical output of shadowed solar arrays. IEEE Transactions on Electron Devices, **18**, 8 DOI 10.1109/T-ED.1971.17231.

Shockley, W., 1949. The theory of p-n junctions in semiconductors and p-n junction transistors. Bell Sys. Tech. J., vol. 28, 435-489.

Thakkar, N., Cormode, D., Lonji, V., Pulver, S., Cronin, A., 2010. A simple non-linear model for the effect of partial shade on PV systems. 35th IEEE Photovoltaic Specialists Conference, Honolulu, HI.

Woyte, A., Nijs, J., Belmans, R., 2003. Partial shadowing of photovoltaic arrays with different system configurations: literature review and field test results. Solar Energy **74**, 217-233.